

# A modified Marchenko method to retrieve the wave field inside a layered metamaterial from reflection measurements at the surface

Kees Wapenaar

*Department of Geoscience and Engineering,*

*Delft University of Technology, 2600 GA Delft, The Netherlands*

(Dated: November 28, 2021)

## Abstract

With the Marchenko method it is possible to retrieve the wave field inside a medium from its reflection response at the surface. To date, this method has predominantly been applied to naturally occurring materials. In this paper we extend the Marchenko method for applications in metamaterials with, in the low-frequency limit, effective negative constitutive parameters. We illustrate the method with a numerical example, which shows that the method works well for vertically propagating plane waves and for dipping plane waves with small horizontal slownesses. The proposed method has potential applications for example in non-destructive testing of layered materials.

PACS numbers: 41.20.Jb, 42.25.Bs, 43.20.+g

## I. INTRODUCTION

Building on classical inverse scattering theory [1–4], recent research has opened new ways of retrieving the wave field inside a medium from its reflection response at the surface [5–13] and using this for imaging [14–22]. These methods, named after Marchenko [1], have in common that they account for multiple scattering inside the medium and yet require only a single-sided reflection response as input, together with a background model of the medium.

To date, the Marchenko method has almost exclusively been applied to naturally occurring materials (with the exception of an application to non-reciprocal materials [23]), but it has not yet been applied to metamaterials with, in the low-frequency limit, effective negative constitutive parameters. A classical reference on wave propagation in materials with negative permittivity and permeability is the paper by Veselago [24], in which it is shown that such materials exhibit negative refraction. Since the discovery by Pendry [25] that negative refraction makes a perfect lens there has been a significant interest in electromagnetic wave propagation in metamaterials [26–34]. Almost simultaneously, after the first fabrication of an elastic metamaterial with effective negative elastic parameters [35], much research has been directed to wave propagation in elastic metamaterials [36–45].

In this paper we modify the Marchenko method for metamaterials. In section II we formulate a unified wave equation that holds for elastodynamic and electromagnetic waves in natural materials and metamaterials. Next, in section III, we derive representations for the Marchenko method for a layered medium, consisting of a mix of natural materials and metamaterials. Using these representations, in section IV we derive the modified Marchenko method, which we illustrate with a numerical example in section V.

## II. UNIFIED WAVE EQUATION

### A. Basic equations

Throughout this paper we consider scalar wave propagation in the 2D plane. This allows capturing different wave phenomena by a unified wave equation. We define the Cartesian coordinate vector in the 2D plane as  $\mathbf{x} = (x_1, x_3)$ , where positive  $x_3$  denotes depth in a horizontally layered medium. Quantities that are a function of space and time are denoted

as  $u(\mathbf{x}, t)$ , where  $t$  stands for time. We define the temporal Fourier transform of  $u(\mathbf{x}, t)$  as

$$u(\mathbf{x}, \omega) = \int_{-\infty}^{\infty} u(\mathbf{x}, t) \exp(i\omega t) dt, \quad (1)$$

where  $\omega$  is the angular frequency and  $i$  the imaginary unit. For convenience, quantities in the time and frequency domain are denoted by the same symbol (here  $u$ ). The inverse Fourier transform is defined as

$$u(\mathbf{x}, t) = \frac{1}{2\pi} \int_{-\infty}^{\infty} u(\mathbf{x}, \omega) \exp(-i\omega t) d\omega. \quad (2)$$

Throughout this paper quantities in the time domain are real-valued, hence, equation (1) implies  $u(\mathbf{x}, -\omega) = u^*(\mathbf{x}, \omega)$ , where the asterisk denotes complex conjugation. Using this property, the inverse Fourier transform can be rewritten as

$$u(\mathbf{x}, t) = \frac{1}{\pi} \Re \int_0^{\infty} u(\mathbf{x}, \omega) \exp(-i\omega t) d\omega, \quad (3)$$

where  $\Re$  denotes that the real part is taken. Since the integral is taken over positive frequencies only, it is sufficient to restrict our derivations in the frequency domain to positive frequencies. This avoids complications related to the sign of the frequency.

In the space-frequency domain, we consider the following system of unified equations in the low-frequency limit for 2D wave propagation in an inhomogeneous, transverse isotropic natural material or metamaterial

$$-i\omega\alpha P + \partial_1 Q_1 + \partial_3 Q_3 = B, \quad (4)$$

$$-i\omega\beta_1 Q_1 + \partial_1 P = C_1, \quad (5)$$

$$-i\omega\beta_3 Q_3 + \partial_3 P = C_3. \quad (6)$$

These equations hold for acoustic (AC), horizontally polarised shear (SH), transverse-electric (TE) and transverse-magnetic (TM) wave fields. Operator  $\partial_i$  stands for the partial differential operator  $\partial/\partial x_i$ . The wave fields [ $P(\mathbf{x}, \omega)$  and  $Q_i(\mathbf{x}, \omega)$ ] and sources [ $B(\mathbf{x}, \omega)$  and  $C_i(\mathbf{x}, \omega)$ ] are space- and frequency-dependent macroscopic quantities. These are often denoted as  $\langle P \rangle$ , etc. [33], but for notational convenience we will not use the brackets. The medium parameters [ $\alpha(x_3, \omega)$  and  $\beta_i(x_3, \omega)$ ] are effective parameters (which, in a layered medium, are varying in the  $x_3$ -direction only). At layer interfaces, where the medium parameters are discontinuous, the unified boundary conditions state that the wave field quantities  $P$  and  $Q_3$  are continuous.

Table 1: Quantities in unified equations (4) to (6).

	$P$	$Q_1$	$Q_3$	$\alpha$	$\beta_1$	$\beta_3$	$B$	$C_1$	$C_3$
AC	$p$	$v_1$	$v_3$	$\kappa$	$\rho_{11}$	$\rho_{33}$	$q$	$F_1$	$F_3$
SH	$v_2$	$-\tau_{21}$	$-\tau_{23}$	$\rho_{22}$	$4s_{1221}$	$4s_{3223}$	$F_2$	$2h_{21}$	$2h_{23}$
TE	$E_2$	$H_3$	$-H_1$	$\varepsilon_{22}$	$\mu_{33}$	$\mu_{11}$	$-J_2^e$	$-J_3^m$	$J_1^m$
TM	$H_2$	$-E_3$	$E_1$	$\mu_{22}$	$\varepsilon_{33}$	$\varepsilon_{11}$	$-J_2^m$	$J_3^e$	$-J_1^e$

The wave fields, sources and medium parameters are specified for the different wave phenomena in Table 1. For AC and SH waves,  $p$  is the acoustic pressure,  $\tau_{ij}$  the stress,  $v_i$  the particle velocity,  $\kappa$  the compressibility,  $\rho_{ij}$  the mass density,  $s_{ijkl}$  the compliance,  $q$  the volume injection-rate density,  $F_i$  the external force density and  $h_{ij}$  the external deformation-rate density. For TE and TM waves,  $E_i$  is the electric field strength,  $H_i$  the magnetic field strength,  $\varepsilon_{ij}$  the permittivity,  $\mu_{ij}$  the permeability,  $J_i^e$  the external electric current density and  $J_i^m$  the external magnetic current density.

For natural materials the real parts of the medium parameters  $\alpha$  and  $\beta_i$  are positive. Such a medium will be called a double-positive (DPS) medium [30]. For metamaterials the real part of one or more of the medium parameters is negative. When both  $\alpha$  and  $\beta_i$  have negative real parts, we speak of a double-negative (DNG) medium [30]. To obey causality, the parameters of a DNG medium are frequency-dependent and complex-valued [28]. The sign of the imaginary parts of these parameters follows from the unified power balance

$$\frac{1}{2} \Re \int_{\mathbb{D}} (C_i^* Q_i + B^* P) d^2 \mathbf{x} = \frac{1}{2} \Re \oint_{\partial \mathbb{D}} P^* Q_i n_i d\mathbf{x} + \frac{\omega}{2} \int_{\mathbb{D}} (\Im(\alpha) |P|^2 + \Im(\beta_i) |Q_i|^2) d^2 \mathbf{x}, \quad (7)$$

where  $\Im$  denotes that the imaginary part is taken, and  $\mathbb{D}$  is an arbitrary spatial domain, enclosed by boundary  $\partial \mathbb{D}$  with outward pointing normal vector  $\mathbf{n} = (n_1, n_3)$ . The left-hand side quantifies the power generated by the sources in  $\mathbb{D}$ , the first term on the right-hand side the power leaving  $\mathbb{D}$  via its boundary and the second term on the right-hand side the dissipated power in  $\mathbb{D}$ . For a passive DNG medium the latter term must be positive, hence the imaginary parts of  $\alpha$  and  $\beta_i$  are positive (and for a passive DPS medium they are positive or zero).

In the following we separate the space- and frequency-dependency of the medium param-

eters, for DPS as well as DNG media, according to

$$\alpha(x_3, \omega) = \alpha_0(x_3)h_\alpha(\omega), \quad (8)$$

$$\beta_i(x_3, \omega) = \beta_{i,0}(x_3)h_\beta(\omega), \quad (9)$$

with positive real-valued  $\alpha_0(x_3)$  and  $\beta_{i,0}(x_3)$ . For DNG media, an often used model for the frequency-dependent functions is the Drude model [26], where

$$h_\alpha(\omega) = 1 - \frac{\omega_\alpha^2}{\omega(\omega + i\Gamma_\alpha)}, \quad (10)$$

$$h_\beta(\omega) = 1 - \frac{\omega_\beta^2}{\omega(\omega + i\Gamma_\beta)}, \quad (11)$$

with small positive real-valued  $\Gamma_\alpha$  and  $\Gamma_\beta$ . Note that  $\Re(h_\alpha) < 0$  for  $\omega^2 < \omega_\alpha^2 - \Gamma_\alpha^2$  and  $\Im(h_\alpha) > 0$  for all positive  $\omega$  (and similar properties for  $h_\beta$ ). Hence, in the low-frequency limit these parameters obey the mentioned conditions for a DNG medium.

In the following we assume that the medium parameters (for DPS and DNG media) are defined by the more general relations (8) and (9). Whenever we use the Drude model for DNG media (equations (10) and (11)) we mention this explicitly.

## B. Matrix-vector wave equation

We reorganise the basic equations (4) to (6) into a matrix-vector wave equation. This wave equation is a suited starting point for the derivation of representations for the Marchenko method in section III.

We define the spatial Fourier transform of a function  $u(x_1, x_3, \omega)$  as

$$\tilde{u}(s_1, x_3, \omega) = \int_{-\infty}^{\infty} u(x_1, x_3, \omega) \exp(-i\omega s_1 x_1) dx_1, \quad (12)$$

with  $s_1$  being the horizontal slowness. This transformation accomplishes a decomposition of the wave field  $u(x_1, x_3, \omega)$  into plane-wave components  $\tilde{u}(s_1, x_3, \omega)$ . We use equation (12) to transform equations (4) to (6) from the space-frequency domain  $(x_1, x_3, \omega)$  to the slowness-depth-frequency domain  $(s_1, x_3, \omega)$ . Differentiations with respect to  $x_1$  thus become multiplications by  $i\omega s_1$ . Eliminating  $\tilde{Q}_1$  from the transformed equations, we obtain the following matrix-vector wave equation [46–52]

$$\partial_3 \tilde{\mathbf{q}} = \tilde{\mathbf{A}} \tilde{\mathbf{q}} + \tilde{\mathbf{d}}, \quad (13)$$

with wave vector  $\tilde{\mathbf{q}}(s_1, x_3, \omega)$  and source vector  $\tilde{\mathbf{d}}(s_1, x_3, \omega)$  defined as

$$\tilde{\mathbf{q}} = \begin{pmatrix} \tilde{P} \\ \tilde{Q}_3 \end{pmatrix} \quad \text{and} \quad \tilde{\mathbf{d}} = \begin{pmatrix} \tilde{C}_3 \\ \tilde{B} + s_1 \tilde{C}_1 / \beta_1 \end{pmatrix} \quad (14)$$

and matrix  $\tilde{\mathbf{A}}(s_1, x_3, \omega)$  defined as

$$\tilde{\mathbf{A}} = \begin{pmatrix} 0 & i\omega\beta_3 \\ i\omega s_3^2 / \beta_3 & 0 \end{pmatrix}, \quad (15)$$

with

$$s_3^2 = \alpha\beta_3 - \eta s_1^2, \quad \text{with} \quad \eta = \beta_3 / \beta_1. \quad (16)$$

Note that vector  $\tilde{\mathbf{q}}$  defined in equation (14) contains the wave field quantities that are continuous at interfaces between layers with different medium parameters. Moreover, these quantities constitute the power flux density  $j$  in the  $x_3$ -direction via  $j = \frac{1}{2} \Re\{\tilde{P}^* \tilde{Q}_3\}$ . In the matrix-vector notation this can be written as

$$j = \frac{1}{4} \tilde{\mathbf{q}}^\dagger \mathbf{K} \tilde{\mathbf{q}}, \quad (17)$$

where  $\dagger$  denotes transposition and complex conjugation and where matrix  $\mathbf{K}$  is defined as

$$\mathbf{K} = \begin{pmatrix} 0 & 1 \\ 1 & 0 \end{pmatrix}. \quad (18)$$

The quantity  $s_3^2$  defined in equation (16) is the square of the vertical phase slowness. Using equations (8) and (9) it can be written as

$$s_3^2 = \frac{1}{c_0^2} h_\alpha h_\beta - \eta_0 s_1^2, \quad (19)$$

with

$$c_0 = (\alpha_0 \beta_{3,0})^{-\frac{1}{2}} \quad \text{and} \quad \eta_0 = \beta_{3,0} / \beta_{1,0}. \quad (20)$$

Since  $h_\alpha$  and  $h_\beta$  are complex-valued functions,  $s_3^2$  is complex-valued as well. Defining  $h_\alpha = h_\alpha^r + ih_\alpha^i$  and  $h_\beta = h_\beta^r + ih_\beta^i$  we may write

$$\Re(s_3^2) = \frac{1}{c_0^2} (h_\alpha^r h_\beta^r - h_\alpha^i h_\beta^i) - \eta_0 s_1^2, \quad (21)$$

$$\Im(s_3^2) = \frac{1}{c_0^2} (h_\alpha^r h_\beta^i + h_\alpha^i h_\beta^r). \quad (22)$$

For DPS media, with  $h_\alpha^r, h_\beta^r, h_\alpha^i, h_\beta^i$  all positive (or zero), we have  $\Im(s_3^2) \geq 0$ . For this situation, Figure 1(a) illustrates  $s_3^2$  in the complex plane for a fixed frequency  $\omega$  and variable  $s_1$ . For DNG media, with  $h_\alpha^r, h_\beta^r$  both negative and  $h_\alpha^i, h_\beta^i$  both positive, we have  $\Im(s_3^2) < 0$ . For this situation  $s_3^2$  is illustrated in the complex plane in Figure 1(b).

### C. Decomposition of matrix-vector wave equation

We reorganise the matrix-vector wave equation into an equation for downgoing and upgoing waves. The eigenvalue decomposition of matrix  $\tilde{\mathbf{A}}(s_1, x_3, \omega)$  reads

$$\tilde{\mathbf{A}} = \tilde{\mathbf{L}}\tilde{\mathbf{\Lambda}}\tilde{\mathbf{L}}^{-1}, \quad (23)$$

with  $\tilde{\mathbf{A}}(s_1, x_3, \omega)$ ,  $\tilde{\mathbf{L}}(s_1, x_3, \omega)$  and  $\{\tilde{\mathbf{L}}(s_1, x_3, \omega)\}^{-1}$  defined as

$$\tilde{\mathbf{A}} = \begin{pmatrix} i\omega s_3 & 0 \\ 0 & -i\omega s_3 \end{pmatrix}, \quad (24)$$

$$\tilde{\mathbf{L}} = \begin{pmatrix} 1 & 1 \\ s_3/\beta_3 & -s_3/\beta_3 \end{pmatrix}, \quad (25)$$

$$\tilde{\mathbf{L}}^{-1} = \frac{1}{2} \begin{pmatrix} 1 & \beta_3/s_3 \\ 1 & -\beta_3/s_3 \end{pmatrix}. \quad (26)$$

The vertical phase slowness  $s_3$ , which is defined as the square-root of  $s_3^2$ , is illustrated in Figures 1(c) and 1(d) for DPS and DNG media, respectively. In both cases there are two square-roots, indicated by the two curves in these figures. In section IID we discuss how to choose the proper square-roots.

We introduce a decomposed field vector  $\tilde{\mathbf{p}}$  and a decomposed source vector  $\tilde{\mathbf{s}}$  via

$$\tilde{\mathbf{q}} = \tilde{\mathbf{L}}\tilde{\mathbf{p}}, \quad (27)$$

$$\tilde{\mathbf{d}} = \tilde{\mathbf{L}}\tilde{\mathbf{s}}, \quad (28)$$

with

$$\tilde{\mathbf{p}} = \begin{pmatrix} \tilde{P}^+ \\ \tilde{P}^- \end{pmatrix}, \quad \tilde{\mathbf{s}} = \begin{pmatrix} \tilde{S}^+ \\ \tilde{S}^- \end{pmatrix}. \quad (29)$$

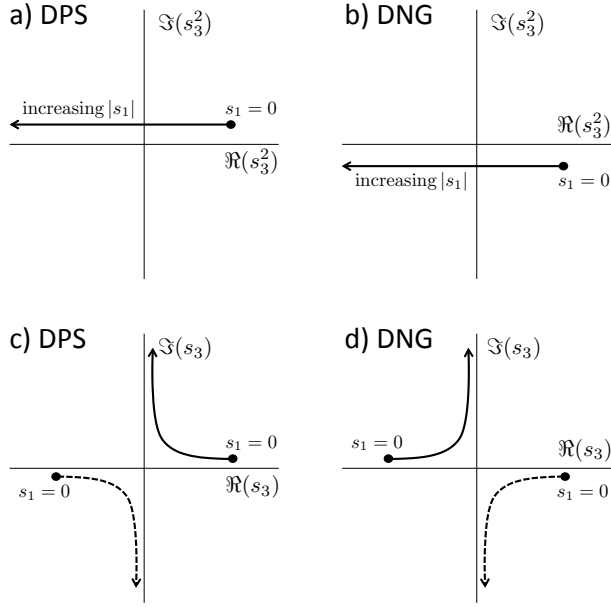


FIG. 1: Squared slowness  $s_3^2$  in the complex plane for (a) DPS and (b) DNG medium. Slowness  $s_3$  in the complex plane for (c) DPS and (d) DNG medium. The solid curves in (c) and (d) represent the proper square-roots of those in (a) and (b).

Substitution of equations (23), (27) and (28) into the matrix-vector wave equation (13) yields

$$\partial_3 \tilde{\mathbf{p}} = (\tilde{\mathbf{\Lambda}} - \tilde{\mathbf{L}}^{-1} \partial_3 \tilde{\mathbf{L}}) \tilde{\mathbf{p}} + \tilde{\mathbf{s}}. \quad (30)$$

This is a coupled system of equations for the downgoing and upgoing wave fields  $\tilde{P}^+$  and  $\tilde{P}^-$ , respectively. We can express the power flux density  $j$  in the  $x_3$ -direction in terms of these wave fields by substituting  $\tilde{\mathbf{q}} = \tilde{\mathbf{L}} \tilde{\mathbf{p}}$  into equation (17). Using equations (18) and (25) we thus obtain

$$\begin{aligned} j &= \frac{1}{4} \tilde{\mathbf{q}}^\dagger \mathbf{K} \tilde{\mathbf{q}} = \frac{1}{4} \tilde{\mathbf{p}}^\dagger \tilde{\mathbf{L}}^\dagger \mathbf{K} \tilde{\mathbf{L}} \tilde{\mathbf{p}} \\ &= \frac{1}{2} \Re(s_3/\beta_3) (|\tilde{P}^+|^2 - |\tilde{P}^-|^2) + \Im(s_3/\beta_3) \Im((\tilde{P}^+)^* \tilde{P}^-). \end{aligned} \quad (31)$$

#### D. Phase slowness

For the discussion on the sign of the vertical phase slowness  $s_3$ , consider an independent downgoing wave field  $\tilde{P}^+$  in a homogeneous medium. For this situation the power flux

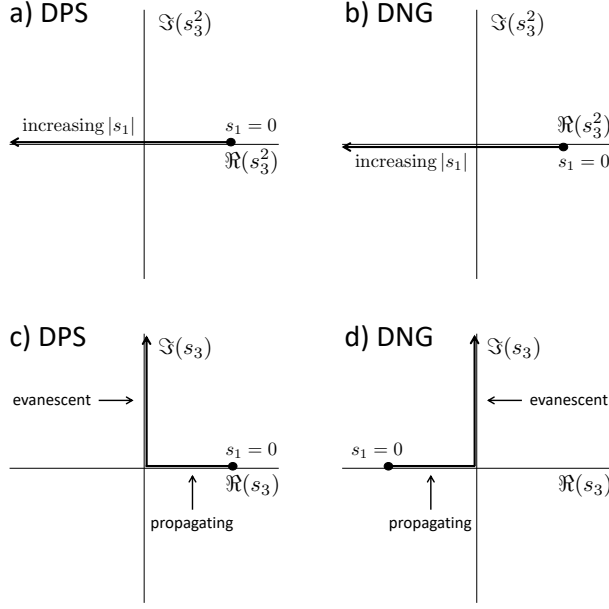


FIG. 2: As Figure 1, for the limiting case of vanishing loss parameters. The curves in (c) and (d) are the proper square-roots of those in (a) and (b).

density can be written as

$$j = \frac{1}{2} \Re(s_3/\beta_3) |\tilde{P}^+|^2 = \frac{h_\beta^r \Re(s_3) + h_\beta^i \Im(s_3)}{2\beta_{3,0} |h_\beta|^2} |\tilde{P}^+|^2, \quad (32)$$

where we used equation (9) to express  $\beta_3$  in terms of the positive quantity  $\beta_{3,0}$  and  $h_\beta = h_\beta^r + ih_\beta^i$ . We now determine the signs of  $\Re(s_3)$  and  $\Im(s_3)$  such that  $\tilde{P}^+$  has a positive power flux density in the positive  $x_3$ -direction [24]. For DPS media, with  $h_\beta^r$  and  $h_\beta^i$  both positive, we find that this condition is fulfilled when  $\Re(s_3) \geq 0$  and  $\Im(s_3) \geq 0$ . Hence, the solid curve in Figure 1(c) represents the proper square-root of  $s_3^2$ . We write this square-root as

$$s_3 = +\sqrt{\frac{1}{c_0^2} h_\alpha h_\beta - \eta_0 s_1^2}, \quad (33)$$

with the + sign in front of the square-root denoting that  $\Re(s_3) \geq 0$ . For DNG media, with  $h_\beta^r$  negative and  $h_\beta^i$  positive, we find that  $j$  is positive when  $\Re(s_3) \leq 0$  and  $\Im(s_3) \geq 0$ . Hence, for this situation the solid curve in Figure 1(d) represents the proper square-root of  $s_3^2$ . We write this square-root as

$$s_3 = -\sqrt{\frac{1}{c_0^2} h_\alpha h_\beta - \eta_0 s_1^2}, \quad (34)$$

with the  $-$  sign in front of the square-root denoting that  $\Re(s_3) \leq 0$ . Equations (33) and (34) express the fact that the vertical phase slowness is positive for DPS media and negative for DNG media. Given these square-roots, we find in the same way that  $j$  is negative for an independent upgoing wave field  $\tilde{P}^-$  in a homogeneous medium.

Figure 2 shows  $s_3^2$  and  $s_3$  in the complex plane for the limiting situation of vanishing losses, i.e., vanishing imaginary parts of the medium parameters. Note that the real and imaginary branches of  $s_3$  correspond to propagating and evanescent waves, respectively.

### E. Group slowness

Despite the fact that the vertical phase slowness in a DNG medium is negative, the vertical group slowness should be positive. This restricts the choice of models for the functions  $h_\alpha(\omega)$  and  $h_\beta(\omega)$ . We define the vertical group slowness as

$$s_3^{\text{gr}} = \Re\left(\frac{\partial(\omega s_3)}{\partial\omega}\right). \quad (35)$$

Substituting equation (34), taking for convenience  $h_\alpha(\omega) = h_\beta(\omega) = h(\omega)$ , we obtain

$$s_3^{\text{gr}} = \Re\left(\frac{h(h + \omega \frac{\partial h}{\partial \omega}) - \eta_0 c_0^2 s_1^2}{c_0^2 s_3}\right). \quad (36)$$

We analyse this expression for the Drude model of equations (10) and (11), with  $\omega_\alpha = \omega_\beta = \omega_0$  and  $\Gamma_\alpha = \Gamma_\beta = \Gamma$ , hence

$$h(\omega) = 1 - \frac{\omega_0^2}{\omega(\omega + i\Gamma)} \quad (37)$$

and

$$h + \omega \partial h / \partial \omega = 1 + \frac{\omega_0^2}{(\omega + i\Gamma)^2}. \quad (38)$$

The condition for a DNG medium,  $\Re(h) < 0$ , requires  $\omega^2 < \omega_0^2 - \Gamma^2$ .

We evaluate the sign of  $s_3^{\text{gr}}$  for two special situations. First we consider vertically propagating waves, i.e.,  $s_1 = 0$ . From equation (34) we find  $s_3 = h/c_0$  for  $\omega^2 < \omega_0^2 - \Gamma^2$ . Using this in equation (36) we obtain [26]

$$s_3^{\text{gr}} = \frac{\Re(h + \omega \partial h / \partial \omega)}{c_0} = \frac{1}{c_0} \Re\left(1 + \frac{\omega_0^2}{(\omega + i\Gamma)^2}\right). \quad (39)$$

Assuming small  $\Gamma$  (a sufficient condition is  $\Gamma < \omega$ ), we find indeed that the vertical group slowness  $s_3^{\text{gr}}$  is positive.

Next we consider non-zero  $s_1$  and analyse equation (36) for the limit  $\Gamma \rightarrow 0$ . From equations (37) and (38) we find  $h = 1 - \omega_0^2/\omega^2$  and  $h(h + \omega\partial h/\partial\omega) = 1 - \omega_0^4/\omega^4$ . Using this in equation (36) we obtain

$$s_3^{\text{gr}} = \frac{\eta_0 c_0^2 s_1^2 + \omega_0^4/\omega^4 - 1}{c_0^2 \sqrt{(\omega_0^2/\omega^2 - 1)^2/c_0^2 - \eta_0 s_1^2}}. \quad (40)$$

For  $\omega < \omega_0$  the nominator is positive for all  $s_1$ . For propagating waves the denominator is real-valued and positive as well, hence  $s_3^{\text{gr}}$  is positive for this situation.

### III. REPRESENTATIONS FOR THE MARCHENKO METHOD

#### A. Propagation invariants for DPS and DNG media

We consider a medium configuration consisting of a homogeneous DPS upper half-space  $x_3 \leq x_{3,0}$  and a horizontally layered lower half-space  $x_3 > x_{3,0}$ , which may consist of an arbitrary mix of DPS and DNG layers. The effective medium parameters in this configuration are  $\alpha(x_3, \omega)$  and  $\beta_i(x_3, \omega)$ . These parameters may vary continuously as a function of  $x_3$  within each layer and jump by a finite amount at layer interfaces. We assume that the losses are small and for the derivation of the Marchenko method we ignore the imaginary parts of  $\alpha(x_3, \omega)$  and  $\beta_i(x_3, \omega)$  (however, in the numerical example in section V we model the input data with complex-valued medium parameters). Assuming that the sources are restricted to the upper half-space  $x_3 \leq x_{3,0}$ , the wave field inside the layers is governed by wave equation (13) with  $\tilde{\mathbf{d}} = \mathbf{0}$ . Moreover,  $\tilde{\mathbf{q}}$  is continuous at layer interfaces. We derive propagation invariants [53–56], which we will use for the derivation of the representations for the Marchenko method in the next section. We consider two independent wave vectors  $\tilde{\mathbf{q}}_A$  and  $\tilde{\mathbf{q}}_B$  and will show that  $\tilde{\mathbf{q}}_A^t \mathbf{N} \tilde{\mathbf{q}}_B$  and  $\tilde{\mathbf{q}}_A^\dagger \mathbf{K} \tilde{\mathbf{q}}_B$  are propagation invariants (i.e., that they are independent of the coordinate  $x_3$  for  $x_3 > x_{3,0}$ ). Here superscript  $t$  denotes transposition and matrix  $\mathbf{N}$  is defined as

$$\mathbf{N} = \begin{pmatrix} 0 & 1 \\ -1 & 0 \end{pmatrix}. \quad (41)$$

Obviously the quantities  $\tilde{\mathbf{q}}_A^t \mathbf{N} \tilde{\mathbf{q}}_B$  and  $\tilde{\mathbf{q}}_A^\dagger \mathbf{K} \tilde{\mathbf{q}}_B$  are continuous at layer interfaces. Hence, to show that these quantities are propagation invariants for the layered medium, it suffices

to show that they are propagation invariants inside a layer. Evaluating  $\partial_3\{\tilde{\mathbf{q}}_A^t\mathbf{N}\tilde{\mathbf{q}}_B\}$  and  $\partial_3\{\tilde{\mathbf{q}}_A^\dagger\mathbf{K}\tilde{\mathbf{q}}_B\}$ , using equation (13) with  $\tilde{\mathbf{d}} = \mathbf{0}$ , we obtain

$$\partial_3\{\tilde{\mathbf{q}}_A^t\mathbf{N}\tilde{\mathbf{q}}_B\} = \tilde{\mathbf{q}}_A^t\tilde{\mathbf{A}}^t\mathbf{N}\tilde{\mathbf{q}}_B + \tilde{\mathbf{q}}_A^t\mathbf{N}\tilde{\mathbf{A}}\tilde{\mathbf{q}}_B, \quad (42)$$

$$\partial_3\{\tilde{\mathbf{q}}_A^\dagger\mathbf{K}\tilde{\mathbf{q}}_B\} = \tilde{\mathbf{q}}_A^\dagger\mathbf{A}^\dagger\mathbf{K}\tilde{\mathbf{q}}_B + \tilde{\mathbf{q}}_A^\dagger\mathbf{K}\tilde{\mathbf{A}}\tilde{\mathbf{q}}_B. \quad (43)$$

Matrix  $\tilde{\mathbf{A}}$ , defined in equation (15), obeys for real-valued medium parameters the following symmetry relations

$$\tilde{\mathbf{A}}^t\mathbf{N} = -\mathbf{N}\tilde{\mathbf{A}}, \quad (44)$$

$$\tilde{\mathbf{A}}^\dagger\mathbf{K} = -\mathbf{K}\tilde{\mathbf{A}}. \quad (45)$$

Hence, the right-hand sides of equations (42) and (43) are equal to zero, which confirms that  $\tilde{\mathbf{q}}_A^t\mathbf{N}\tilde{\mathbf{q}}_B$  and  $\tilde{\mathbf{q}}_A^\dagger\mathbf{K}\tilde{\mathbf{q}}_B$  are propagation invariants.

Next, we derive propagation invariants for decomposed wave fields. Consider two independent decomposed wave vectors  $\tilde{\mathbf{p}}_A$  and  $\tilde{\mathbf{p}}_B$ , which are related to  $\tilde{\mathbf{q}}_A$  and  $\tilde{\mathbf{q}}_B$ , respectively, via equation (27). We obtain propagation invariants for these decomposed wave vectors by substituting  $\tilde{\mathbf{q}}_A = \tilde{\mathbf{L}}\tilde{\mathbf{p}}_A$  and  $\tilde{\mathbf{q}}_B = \tilde{\mathbf{L}}\tilde{\mathbf{p}}_B$  into the propagation invariants  $\tilde{\mathbf{q}}_A^t\mathbf{N}\tilde{\mathbf{q}}_B$  and  $\tilde{\mathbf{q}}_A^\dagger\mathbf{K}\tilde{\mathbf{q}}_B$ . Using equations (18), (25) and (41), we obtain

$$\tilde{\mathbf{q}}_A^t\mathbf{N}\tilde{\mathbf{q}}_B = \tilde{\mathbf{p}}_A^t\tilde{\mathbf{L}}^t\mathbf{N}\tilde{\mathbf{L}}\tilde{\mathbf{p}}_B = -2(s_3/\beta_3)\tilde{\mathbf{p}}_A^t\mathbf{N}\tilde{\mathbf{p}}_B \quad (46)$$

and

$$\tilde{\mathbf{q}}_A^\dagger\mathbf{K}\tilde{\mathbf{q}}_B = \tilde{\mathbf{p}}_A^\dagger\tilde{\mathbf{L}}^\dagger\mathbf{K}\tilde{\mathbf{L}}\tilde{\mathbf{p}}_B = 2\tilde{\mathbf{p}}_A^\dagger(\Re(s_3/\beta_3)\mathbf{J} - i\Im(s_3/\beta_3)\mathbf{N})\tilde{\mathbf{p}}_B, \quad (47)$$

with

$$\mathbf{J} = \begin{pmatrix} 1 & 0 \\ 0 & -1 \end{pmatrix}. \quad (48)$$

From equations (29), (41) and (46) we obtain the propagation invariant

$$(s_3/\beta_3)(\tilde{P}_A^+\tilde{P}_B^- - \tilde{P}_A^-\tilde{P}_B^+). \quad (49)$$

From equations (29), (47) and (48) we obtain for propagating waves (i.e., for real-valued  $s_3$ ) the propagation invariant

$$(s_3/\beta_3)((\tilde{P}_A^+)^*\tilde{P}_B^+ - (\tilde{P}_A^-)^*\tilde{P}_B^-). \quad (50)$$

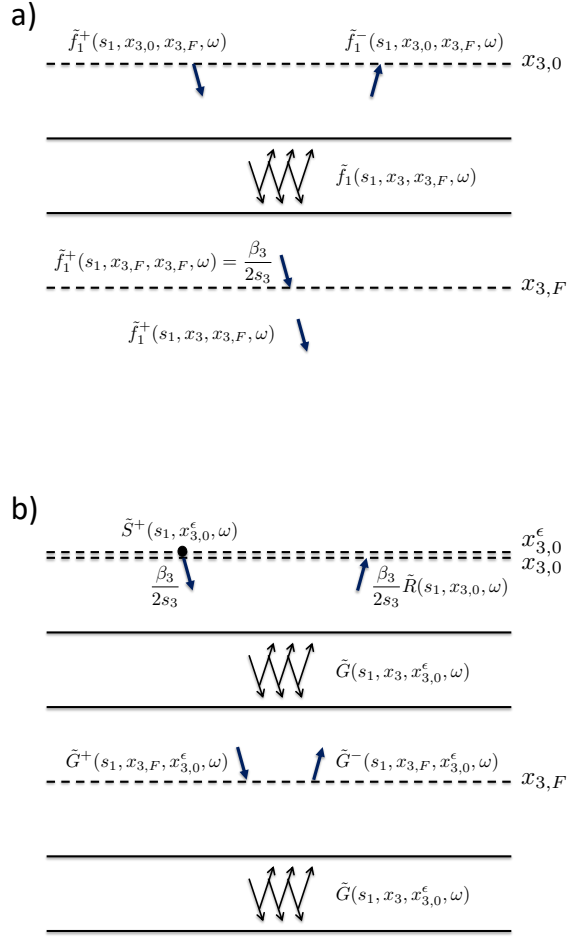


FIG. 3: (a) The focusing function  $\tilde{f}_1 = \tilde{f}_1^+ + \tilde{f}_1^-$ , defined in a truncated version of the actual medium. (b) The Green's function  $\tilde{G} = \tilde{G}^+ + \tilde{G}^-$ , defined in the actual medium.

## B. Representations

We use the propagation invariants of equations (49) and (50) to derive representations for the Marchenko method. We introduce decomposed focusing functions (Figure 3(a)) and Green's functions (Figure 3(b)) and derive relations between them using (49) and (50), with  $\tilde{P}_A^\pm$  and  $\tilde{P}_B^\pm$  replaced by the focusing functions and Green's functions, respectively [14, 15].

First we discuss the Green's functions. For the source quantities in equation (14) we take  $\tilde{B}(s_1, x_3, \omega) = \delta(x_3 - x_{3,0}^\epsilon)$  and  $\tilde{C}_i(s_1, x_3, \omega) = 0$ , where  $x_{3,0}^\epsilon = x_{3,0} - \epsilon$ , with  $\epsilon$  a vanishing positive constant, so that the source of the Green's function is located in the homogeneous upper half-space, just above  $x_{3,0}$  (Figure 3(b)). For the wave field  $\tilde{P}$  in equation (14) we take  $\tilde{P} = \tilde{G}(s_1, x_3, x_{3,0}^\epsilon, \omega)$ , with  $x_{3,0}^\epsilon$  and  $x_3$  denoting the source and receiver coordinates of

the Green's function. We decompose the Green's function at the receiver position  $x_3$  into downgoing and upgoing components  $\tilde{P}^+ = \tilde{G}^+(s_1, x_3, x_{3,0}^\epsilon, \omega)$  and  $\tilde{P}^- = \tilde{G}^-(s_1, x_3, x_{3,0}^\epsilon, \omega)$ , respectively. According to equations (14), (25), (27) and (29), these components are related to the total Green's function  $\tilde{P} = \tilde{G}(s_1, x_3, x_{3,0}^\epsilon, \omega)$  via

$$\tilde{G} = \tilde{G}^+ + \tilde{G}^-. \quad (51)$$

Furthermore, according to equations (14), (26), (28) and (29), the decomposed Green's sources are related to the total Green's source  $\tilde{B}(s_1, x_3, \omega) = \delta(x_3 - x_{3,0}^\epsilon)$  via

$$\tilde{S}^\pm(s_1, x_3, \omega) = \pm(\beta_3/2s_3)\delta(x_3 - x_{3,0}^\epsilon). \quad (52)$$

The source  $\tilde{S}^-$  radiates upgoing waves into the homogeneous half-space above  $x_{3,0}^\epsilon$ , which will not return into the layered medium and will therefore not be further considered. The source  $\tilde{S}^+$  radiates downgoing waves into the medium below  $x_{3,0}^\epsilon$ . Due to scattering in the layered medium, the field at any depth  $x_3 > x_{3,0}^\epsilon$  consists of the downgoing and upgoing components  $\tilde{G}^+(s_1, x_3, x_{3,0}^\epsilon, \omega)$  and  $\tilde{G}^-(s_1, x_3, x_{3,0}^\epsilon, \omega)$ . At  $x_3 = x_{3,0}$ , i.e., at a vanishing distance  $\epsilon$  below the source, the downgoing component reads

$$\tilde{G}^+(s_1, x_{3,0}, x_{3,0}^\epsilon, \omega) = (\beta_3/2s_3) \lim_{\epsilon \rightarrow 0} \exp\{i\omega s_3 \epsilon\} = \frac{\beta_3(x_{3,0}, \omega)}{2s_3(s_1, x_{3,0}, \omega)}. \quad (53)$$

This follows from equations (24), (29), (30) and (52), taking into account that the medium between  $x_{3,0}^\epsilon$  and  $x_{3,0}$  is homogeneous. At the same depth level ( $x_3 = x_{3,0}$ ) we relate the upgoing component to the reflection response  $\tilde{R}(s_1, x_{3,0}, \omega)$  of the layered medium, via

$$\tilde{G}^-(s_1, x_{3,0}, x_{3,0}^\epsilon, \omega) = \frac{\beta_3(x_{3,0}, \omega)\tilde{R}(s_1, x_{3,0}, \omega)}{2s_3(s_1, x_{3,0}, \omega)}, \quad (54)$$

where the factor  $\beta_3/2s_3$  is introduced for convenience, to compensate for the source properties expressed by equation (52). The decomposed Green's functions  $\tilde{G}^+$  and  $\tilde{G}^-$  will be substituted for  $\tilde{P}_B^+$  and  $\tilde{P}_B^-$  in the propagation invariants of equations (49) and (50). Table 2 shows these functions at depth level  $x_3 = x_{3,0}$  (just below the source) and at an arbitrary depth level  $x_3 = x_{3,F}$  (with  $x_{3,F} > x_{3,0}$ ) inside the layered medium. Note that for convenience we dropped the superscript  $\epsilon$  from  $x_{3,0}^\epsilon$ .

Table 2: Quantities used in the propagation invariants of equations (49) and (50).

	$\tilde{P}_A^+(s_1, x_3, \omega)$	$\tilde{P}_A^-(s_1, x_3, \omega)$	$\tilde{P}_B^+(s_1, x_3, \omega)$	$\tilde{P}_B^-(s_1, x_3, \omega)$
$x_3 = x_{3,0}$	$\tilde{f}_1^+(s_1, x_{3,0}, x_{3,F}, \omega)$	$\tilde{f}_1^-(s_1, x_{3,0}, x_{3,F}, \omega)$	$\frac{\beta_3(x_{3,0}, \omega)}{2s_3(s_1, x_{3,0}, \omega)}$	$\frac{\beta_3(x_{3,0}, \omega)\tilde{R}(s_1, x_{3,0}, \omega)}{2s_3(s_1, x_{3,0}, \omega)}$
$x_3 = x_{3,F}$	$\frac{\beta_3(x_{3,F}, \omega)}{2s_3(s_1, x_{3,F}, \omega)}$	0	$\tilde{G}^+(s_1, x_{3,F}, x_{3,0}, \omega)$	$\tilde{G}^-(s_1, x_{3,F}, x_{3,0}, \omega)$

Next we discuss the focusing functions [57]. We define these functions in a truncated version of the actual medium (Figure 3(a)). This truncated medium is taken identical to the actual medium above  $x_3 = x_{3,F}$  and homogeneous below this depth level. We call  $x_{3,F}$  the focal depth. Analogous to equation (51) we define the focusing function  $\tilde{f}_1(s_1, x_3, x_{3,F}, \omega)$  as a superposition of downgoing and upgoing components  $\tilde{f}_1^+(s_1, x_3, x_{3,F}, \omega)$  and  $\tilde{f}_1^-(s_1, x_3, x_{3,F}, \omega)$ , respectively, according to

$$\tilde{f}_1 = \tilde{f}_1^+ + \tilde{f}_1^-. \quad (55)$$

The downgoing focusing function  $\tilde{f}_1^+(s_1, x_{3,0}, x_{3,F}, \omega)$  is incident to the truncated layered medium from the upper boundary  $x_{3,0}$  and is designed such that  $\tilde{f}_1^+(s_1, x_{3,F}, x_{3,F}, \omega)$  focuses at the focal depth  $x_{3,F}$ . Inside the medium scattering takes place and the upgoing focusing function  $\tilde{f}_1^-(s_1, x_{3,0}, x_{3,F}, \omega)$  reaches the upper boundary  $x_{3,0}$ . Below the focal depth  $x_{3,F}$  the focusing function continues propagating downward into the homogeneous lower half-space of the truncated medium. We define  $\tilde{T}(s_1, x_{3,F}, x_{3,0}, \omega)$  as the transmission response of the truncated medium between  $x_{3,0}$  and  $x_{3,F}$ . Hence, the propagation of the focusing function from  $x_{3,0}$  to  $x_{3,F}$  is described by

$$\tilde{f}_1^+(s_1, x_{3,F}, x_{3,F}, \omega) = \tilde{T}(s_1, x_{3,F}, x_{3,0}, \omega)\tilde{f}_1^+(s_1, x_{3,0}, x_{3,F}, \omega). \quad (56)$$

The left-hand side describes the focused field at  $x_{3,F}$ . We could define this as  $\tilde{f}_1^+(s_1, x_{3,F}, x_{3,F}, \omega) = 1$  (with the inverse Fourier transform of 1 being a temporal delta

function). However, in analogy with the Green's function at the source depth in equation (53), we define the focused field at the focal depth as

$$\tilde{f}_1^+(s_1, x_{3,F}, x_{3,F}, \omega) = \frac{\beta_3(x_{3,F}, \omega)}{2s_3(s_1, x_{3,F}, \omega)}. \quad (57)$$

From equations (56) and (57) it follows that the downgoing focusing function  $\tilde{f}_1^+(s_1, x_3, x_{3,F}, \omega)$  for  $x_3 = x_{3,0}$  is related to the transmission response of the truncated medium via

$$\tilde{f}_1^+(s_1, x_{3,0}, x_{3,F}, \omega) = \frac{\beta_3(x_{3,F}, \omega)}{2s_3(s_1, x_{3,F}, \omega)\tilde{T}(s_1, x_{3,F}, x_{3,0}, \omega)}. \quad (58)$$

Since the truncated medium is homogeneous below the focal depth there is no upgoing field at the focal depth, hence

$$\tilde{f}_1^-(s_1, x_{3,F}, x_{3,F}, \omega) = 0. \quad (59)$$

The decomposed focusing functions  $\tilde{f}_1^+$  and  $\tilde{f}_1^-$  will be substituted for  $\tilde{P}_A^+$  and  $\tilde{P}_A^-$  in the propagation invariants of equations (49) and (50). Table 2 shows these functions at depth levels  $x_3 = x_{3,0}$  and  $x_3 = x_{3,F}$ . An underlying assumption for the propagation invariants is that the fields  $\tilde{P}_A^\pm$  and  $\tilde{P}_B^\pm$  are defined in the same source-free medium. This condition is fulfilled in the region between  $x_{3,0}$  and  $x_{3,F}$ . Substituting the quantities of Table 2 into the propagation invariant of equation (49) and equating the results for  $x_{3,0}$  and  $x_{3,F}$  yields

$$\tilde{G}^-(s_1, x_{3,F}, x_{3,0}, \omega) + \tilde{f}_1^-(s_1, x_{3,0}, x_{3,F}, \omega) = \tilde{R}(s_1, x_{3,0}, \omega)\tilde{f}_1^+(s_1, x_{3,0}, x_{3,F}, \omega). \quad (60)$$

In a similar way we obtain from the propagation invariant of equation (50) for propagating waves

$$\tilde{G}^+(s_1, x_{3,F}, x_{3,0}, \omega) - \{\tilde{f}_1^+(s_1, x_{3,0}, x_{3,F}, \omega)\}^* = -\tilde{R}(s_1, x_{3,0}, \omega)\{\tilde{f}_1^-(s_1, x_{3,0}, x_{3,F}, \omega)\}^*. \quad (61)$$

These representations express the downgoing and upgoing components of the Green's function at an arbitrarily chosen depth level  $x_3 = x_{3,F}$  in terms of the reflection response at the surface  $x_3 = x_{3,0}$  and decomposed focusing functions. These representations hold for a layered medium with an arbitrary mix of DPS and DNG layers. The reflection response  $\tilde{R}(s_1, x_{3,0}, \omega)$  can be obtained from measurements at the surface  $x_{3,0}$ . According to equation

(58), the focusing function  $\tilde{f}_1^+(s_1, x_{3,0}, x_{3,F}, \omega)$  could in principle be obtained from the transmission response of the truncated medium. However, this would require detailed knowledge of the medium between  $x_{3,0}$  and  $x_{3,F}$ . In the next section we discuss the Marchenko method, which enables retrieving the focusing functions from the reflection response at the surface and a background model of the medium.

#### IV. THE MARCHENKO METHOD

We start by transforming the representations of equations (60) and (61) to the time domain. Analogous to equation (3), we define the following inverse Fourier transform

$$u(s_1, x_3, \tau) = \frac{1}{\pi} \Re \int_0^\infty \tilde{u}(s_1, x_3, \omega) \exp(-i\omega\tau) d\omega, \quad (62)$$

where  $\tau$  is the so-called intercept time [58]. Applying this inverse transform to equations (60) and (61), we obtain

$$\begin{aligned} & G^-(s_1, x_{3,F}, x_{3,0}, \tau) + f_1^-(s_1, x_{3,0}, x_{3,F}, \tau) \\ &= \int_{-\infty}^\tau R(s_1, x_{3,0}, \tau - \tau') f_1^+(s_1, x_{3,0}, x_{3,F}, \tau') d\tau' \end{aligned} \quad (63)$$

and

$$\begin{aligned} & G^+(s_1, x_{3,F}, x_{3,0}, \tau) - f_1^+(s_1, x_{3,0}, x_{3,F}, -\tau) \\ &= - \int_{-\infty}^\tau R(s_1, x_{3,0}, \tau - \tau') f_1^-(s_1, x_{3,0}, x_{3,F}, -\tau') d\tau'. \end{aligned} \quad (64)$$

For the derivation of the Marchenko method we need time windows that suppress the Green's functions on the left-hand sides of representations (63) and (64), so that we are left with two equations for the two focusing functions. First we briefly review these windows for the situation of a layered medium consisting of DPS layers only. Figure 4 shows an example of the functions in the left-hand sides of equations (63) and (64) for such a medium. Note that these functions (represented by the solid lines) have been convolved with a symmetric band-limited wavelet. Figures 4(a) and (b) show the functions in the left-hand side of equation (64). The direct arrival of the downgoing Green's function  $G^+(s_1, x_{3,F}, x_{3,0}, \tau)$  in Figure 4(a) coincides with the time-reversed direct arrival of the focusing function  $f_1^+(s_1, x_{3,0}, x_{3,F}, \tau)$  in Figure 4(b). For this focusing function we write

$$f_1^+(s_1, x_{3,0}, x_{3,F}, \tau) = f_{1,d}^+(s_1, x_{3,0}, x_{3,F}, \tau) + M^+(s_1, x_{3,0}, x_{3,F}, \tau), \quad (65)$$

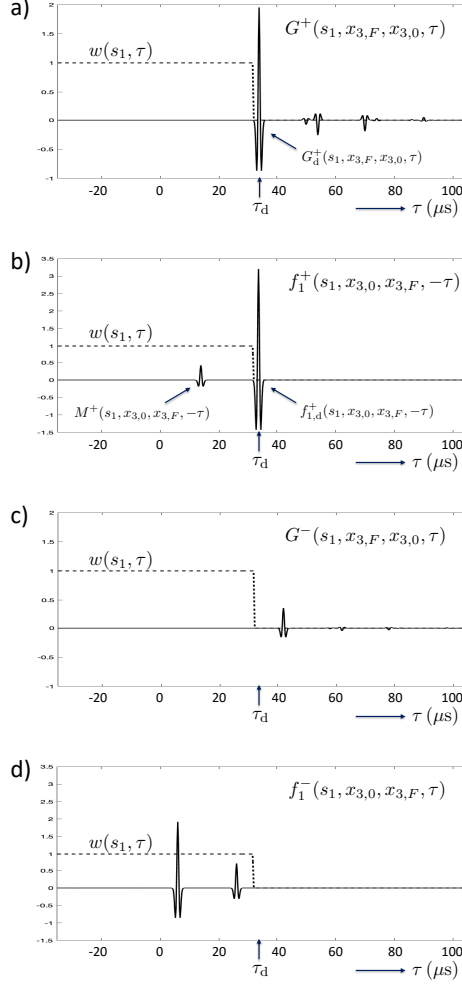


FIG. 4: *The Green's functions and focusing functions in the left-hand sides of equations (63) and (64), for the situation of a layered medium consisting of DPS layers only. The time window  $w(s_1, \tau)$ , indicated by the dashed lines, is the same for all functions.*

where  $f_{1,d}^+$  is the direct arrival and  $M^+$  a coda, following the direct arrival (in Figure 4(b) this coda is time-reversed and consists of a single event only, but more generally it consists of multiple events). We define a time window  $w(s_1, \tau) = \theta(\tau_d(s_1) - \tau_\epsilon - \tau)$ , where  $\theta(\tau)$  is the Heaviside step function,  $\tau_d(s_1)$  the traveltime of the direct arrival of the downgoing Green's function and  $\tau_\epsilon$  is half the duration of the symmetric wavelet. This window is indicated by the dashed lines in Figures 4(a) and (b). It suppresses the downgoing Green's function in Figure 4(a) and the time-reversed direct arrival of the focusing function in Figure 4(b). It passes the time-reversed coda  $M^+(s_1, x_{3,0}, x_{3,F}, -\tau)$  in Figure 4(b). Figures 4(c) and (d) show the functions in the left-hand side of equation (63). Since the first arrival of the upgoing Green's

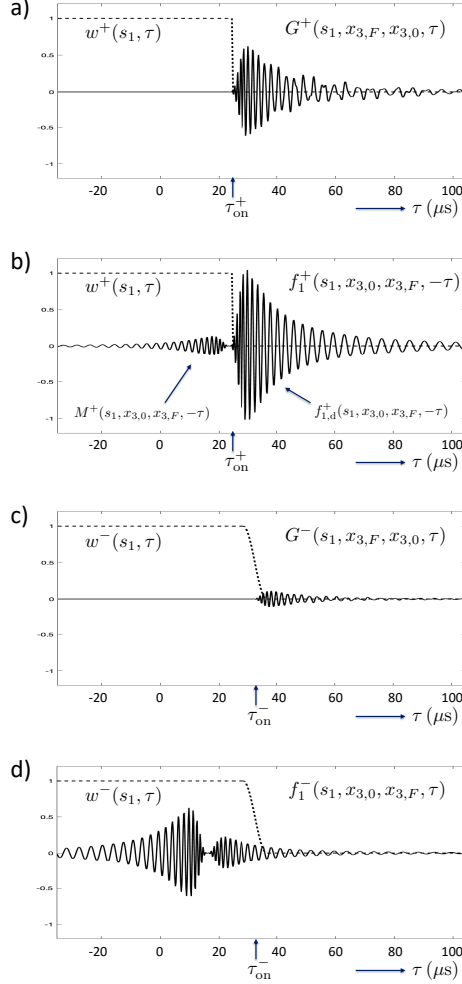


FIG. 5: As Figure 4, but for the situation of a layered medium consisting of DPS and DNG layers. Note the different time windows  $w^+(s_1, \tau)$  and  $w^-(s_1, \tau)$ , indicated by the dashed lines.

function  $G^-(s_1, x_{3,F}, x_{3,0}, \tau)$  arrives later than that of the downgoing Green's function, the time window  $w(s_1, \tau)$  suppresses the upgoing Green's function in Figure 4(c). It passes the focusing function  $f_1^-(s_1, x_{3,0}, x_{3,F}, \tau)$  in Figure 4(d). Applying the window to both sides of equations (63) and (64), the windowed equations can be solved for  $f_1^-(s_1, x_{3,0}, x_{3,F}, \tau)$  and  $M^+(s_1, x_{3,0}, x_{3,F}, \tau)$ , after which the Green's functions follow from the unwinded equations [14, 15].

Next we discuss the time windows for the situation of a layered medium consisting of a mix of DPS and DNG layers. Figures 5(a) and (b) show an example of the functions in the left-hand side of equation (64) (again convolved with a symmetric band-limited wavelet). Due to the highly dispersive character of the DNG layers, these functions are very different

from their counterparts in Figures 4(a) and (b). Nevertheless, for the focusing function  $f_1^+(s_1, x_{3,0}, x_{3,F}, \tau)$  we can again distinguish between a direct arrival  $f_{1,d}^+$  and a coda  $M^+$ , see Figure 5(b) and equation (65). We define a time window

$$w^+(s_1, \tau) = \theta(\tau_{\text{on}}^+(s_1) - \tau), \quad (66)$$

where  $\tau_{\text{on}}^+(s_1)$  is the travelttime of the onset of the downgoing Green's function. This window suppresses the downgoing Green's function in Figure 5(a) and the time-reversed direct arrival of the focusing function in Figure 5(b); it passes the time-reversed coda  $M^+(s_1, x_{3,0}, x_{3,F}, -\tau)$  in Figure 5(b). Figures 5(c) and (d) show the functions in the left-hand side of equation (63). The onset time  $\tau_{\text{on}}^-(s_1)$  of the upgoing Green's function in Figure 5(c) is larger than that of the downgoing Green's function. Note, however, that  $f_1^-(s_1, x_{3,0}, x_{3,F}, \tau)$  in Figure 5(d) exceeds not only the onset time of the downgoing Green's function but also that of the upgoing Green's function. Hence, the upgoing Green's function in Figure 5(c) and the focusing function in Figure 5(d) cannot be uniquely separated by a time window. We define a time window

$$w^-(s_1, \tau) = \theta_{\text{tap}}(\tau_{\text{on}}^-(s_1) - \tau), \quad (67)$$

where  $\theta_{\text{tap}}(\tau)$  is a tapered step function. It is indicated by the dashed lines in Figures 5(c) and 5(d). The taper should be chosen such that this window suppresses the upgoing Green's function in Figure 5(c) as good as possible and leaves the focusing function  $f_1^-(s_1, x_{3,0}, x_{3,F}, \tau)$  in Figure 5(d) as much as possible intact. It is unavoidable that this approach leads to approximations, particularly in the situation of thin layers.

Assuming a proper window function  $w^-(s_1, \tau)$  can be found, the application of this window to both sides of equation (63), and window  $w^+(s_1, \tau)$  to both sides of equation (64), yields the following system of coupled Marchenko equations for  $f_1^-(s_1, x_{3,0}, x_{3,F}, \tau)$  and  $M^+(s_1, x_{3,0}, x_{3,F}, \tau)$

$$f_1^-(s_1, x_{3,0}, x_{3,F}, \tau) = w^-(s_1, \tau) \int_{-\infty}^{\tau} R(s_1, x_{3,0}, \tau - \tau') f_1^+(s_1, x_{3,0}, x_{3,F}, \tau') d\tau' \quad (68)$$

and

$$M^+(s_1, x_{3,0}, x_{3,F}, -\tau) = w^+(s_1, \tau) \int_{-\infty}^{\tau} R(s_1, x_{3,0}, \tau - \tau') f_1^-(s_1, x_{3,0}, x_{3,F}, -\tau') d\tau', \quad (69)$$

with  $f_1^+(s_1, x_{3,0}, x_{3,F}, \tau)$  defined in equation (65). This system of equations can be solved by the following iterative scheme

$$f_{1,k}^-(s_1, x_{3,0}, x_{3,F}, \tau) = w^-(s_1, \tau) \int_{-\infty}^{\tau} R(s_1, x_{3,0}, \tau - \tau') f_{1,k}^+(s_1, x_{3,0}, x_{3,F}, \tau') d\tau' \quad (70)$$

and

$$M_{k+1}^+(s_1, x_{3,0}, x_{3,F}, -\tau) = w^+(s_1, \tau) \int_{-\infty}^{\tau} R(s_1, x_{3,0}, \tau - \tau') f_{1,k}^-(s_1, x_{3,0}, x_{3,F}, -\tau') d\tau', \quad (71)$$

with

$$f_{1,k}^+(s_1, x_{3,0}, x_{3,F}, \tau) = f_{1,d}^+(s_1, x_{3,0}, x_{3,F}, \tau) + M_k^+(s_1, x_{3,0}, x_{3,F}, \tau), \quad (72)$$

starting with  $M_1^+(s_1, x_{3,0}, x_{3,F}, \tau) = 0$ . Note that this scheme requires the measured reflection response  $R(s_1, x_{3,0}, \tau)$  of the layered medium, estimates of the onset times  $\tau_{\text{on}}^+(s_1)$  and  $\tau_{\text{on}}^-(s_1)$ , and an estimate of the direct arrival of the focusing function,  $f_{1,d}^+(s_1, x_{3,0}, x_{3,F}, \tau)$ . Assuming a background model of the medium is available, the primary downgoing and upgoing waves can be modelled, from which the onset times can be retrieved. Moreover, the direct arrival of the focusing function can be obtained, analogous to equation (58), from the direct arrival of the transmission response  $\tilde{T}_d(s_1, x_{3,F}, x_{3,0}, \omega)$  (i.e., the modelled primary downgoing wave), according to

$$\tilde{f}_{1,d}^+(s_1, x_{3,0}, x_{3,F}, \omega) = \frac{\beta_3(x_{3,F}, \omega)}{2s_3(s_1, x_{3,F}, \omega) \tilde{T}_d(s_1, x_{3,F}, x_{3,0}, \omega)}, \quad (73)$$

followed by an inverse Fourier transform.

Once the iterative scheme has converged, the retrieved focusing functions can be used in representations (63) and (64) to obtain the decomposed Green's functions  $G^-(s_1, x_{3,F}, x_{3,0}, \tau)$  and  $G^+(s_1, x_{3,F}, x_{3,0}, \tau)$  and, finally, the total Green's function  $G(s_1, x_{3,F}, x_{3,0}, \tau) = G^+(s_1, x_{3,F}, x_{3,0}, \tau) + G^-(s_1, x_{3,F}, x_{3,0}, \tau)$ . Note that the latter can be interpreted as the response to a source at the surface  $x_{3,0}$ , observed by a virtual receiver at  $x_{3,F}$  inside the medium. Using reciprocity,  $G(s_1, x_{3,0}, x_{3,F}, \tau)$  can be interpreted as the response to a virtual source at  $x_{3,F}$  inside the medium, observed by a receiver at  $x_{3,0}$ . The retrieved Green's function contains the direct arrival and the primary and multiple reflections of the layered medium. The direct arrival comes from the background model whereas the primary and multiple reflections come from the measured reflection response at the surface.

Next, we show how to obtain the response between a virtual source and a virtual receiver, both inside the medium. To this end, note that the decomposed Green's functions are mutually related via[59, 60]

$$G^-(s_1, x_{3,F}, x_{3,0}, \tau) = \int_{-\infty}^{\tau} R(s_1, x_{3,F}, \tau - \tau')G^+(s_1, x_{3,F}, x_{3,0}, \tau')d\tau', \quad (74)$$

where  $R(s_1, x_{3,F}, \tau)$  is the reflection response at depth level  $x_{3,F}$  of the medium below this depth level, assuming a homogeneous medium above this depth level. By inverting equation (74), which is done by deconvolution,  $R(s_1, x_{3,F}, \tau)$  is obtained from  $G^-(s_1, x_{3,F}, x_{3,0}, \tau)$  and  $G^+(s_1, x_{3,F}, x_{3,0}, \tau)$ . This deconvolution process removes all the multiple reflections occurring in the medium above  $x_{3,F}$ . The retrieved reflection response  $R(s_1, x_{3,F}, \tau)$  can be interpreted as the response to a virtual source for downgoing waves at  $x_{3,F}$ , observed by a virtual receiver for upgoing waves at  $x_{3,F}$ .

## V. NUMERICAL EXAMPLE

We illustrate the Marchenko method with a numerical example for a horizontally layered acoustic medium consisting of a mix of DPS and DNG layers, see Figure 6. All layers are homogeneous and isotropic, with  $\beta_1 = \beta_3 = \beta$ , where  $\beta$  stands for the mass density (see Table 1).

The DPS layers consist of natural non-dispersive materials, with  $h_\alpha(\omega) = h_\beta(\omega) = 1$ . Hence, according to equations (8) and (9), the layer parameters simplify to  $\alpha(\omega) = \alpha_0$  and  $\beta(\omega) = \beta_0$ . In Figure 6, the parameters of the DPS layers are the mass density  $\beta_0$  and the phase velocity  $c_0 = (\alpha_0\beta_0)^{-\frac{1}{2}}$ .

The DNG layers consist of dispersive metamaterials. For these layers we use the Drude model of equations (10) and (11), with  $\omega_\alpha = \omega_\beta = \omega_0$  and  $\Gamma_\alpha = \Gamma_\beta = \Gamma$ . Hence,  $h_\alpha(\omega) = h_\beta(\omega) = h(\omega) = 1 - \frac{\omega_0^2}{\omega(\omega+i\Gamma)}$ . For low frequencies ( $\omega \ll \omega_0$ ) this is approximated by  $h(\omega) = -\frac{\omega_0^2}{\omega(\omega+i\Gamma)}$ . Using equations (8) and (9), we write

$$\alpha(\omega) = \alpha_0 h(\omega) = \bar{\alpha}_0 \bar{h}(\omega), \quad (75)$$

$$\beta(\omega) = \beta_0 h(\omega) = \bar{\beta}_0 \bar{h}(\omega), \quad (76)$$

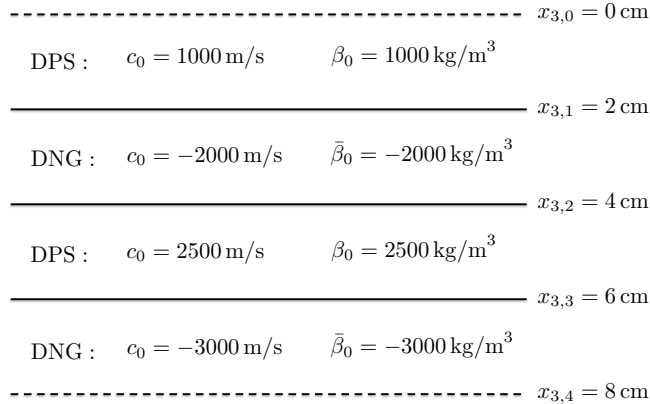


FIG. 6: *Layered acoustic medium, consisting of DPS and DNG layers.*

with

$$\bar{\alpha}_0 = -\alpha_0 \frac{\omega_0^2}{\omega_c^2} < 0, \quad (77)$$

$$\bar{\beta}_0 = -\beta_0 \frac{\omega_0^2}{\omega_c^2} < 0, \quad (78)$$

$$\bar{h}(\omega) = -h(\omega) \frac{\omega_c^2}{\omega_0^2} = \frac{\omega_c^2}{\omega(\omega + i\Gamma)}, \quad (79)$$

where  $\omega_c$  is the central angular frequency of the wave fields that will be considered. For consistency with the low frequency assumption, we assume  $\omega_c \ll \omega_0$ . In Figure 6, the parameters of the DNG layers are the mass density  $\bar{\beta}_0$  and the phase velocity  $c_0 = -(\bar{\alpha}_0 \bar{\beta}_0)^{-\frac{1}{2}}$ . The parameter  $\Gamma$  in the DNG layers is set to  $\Gamma = \omega_c/1000$ .

We consider a band-limited ultrasonic downgoing plane wave, incident to the layered medium at  $x_{3,0} = 0$  cm. The source function of the incident wave is defined as  $S(\tau) = (1 - 2\pi^2 f_c^2 \tau^2) \exp(-\pi^2 f_c^2 \tau^2)$  (a so-called Ricker wavelet), with a central frequency  $f_c = \omega_c/2\pi = 500$  kHz. We use a wavenumber-frequency domain modelling method [61], adjusted for metamaterials, to model the response to this plane wave. For the moment we consider vertically propagating plane waves, hence, we take  $s_1 = 0$ . The modelled reflection response  $R(s_1 = 0, x_{3,0}, \tau)$ , convolved with the wavelet  $S(\tau)$ , is shown in Figure 7(a). This figure clearly shows the non-dispersed reflection at  $40 \mu\text{s}$  from the first layer interface at  $x_{3,1} = 2$  cm. It also shows the dispersed reflections from deeper interfaces, including multiple reflections between the interfaces. Figure 7(b) is the modelled Green's function  $G(s_1 = 0, x_3, x_{3,0}, \tau)$  inside the medium, as a function of depth  $x_3$  and time  $\tau$ . This serves as a reference for the results we will obtain with the Marchenko method. To make the later arrivals visible,

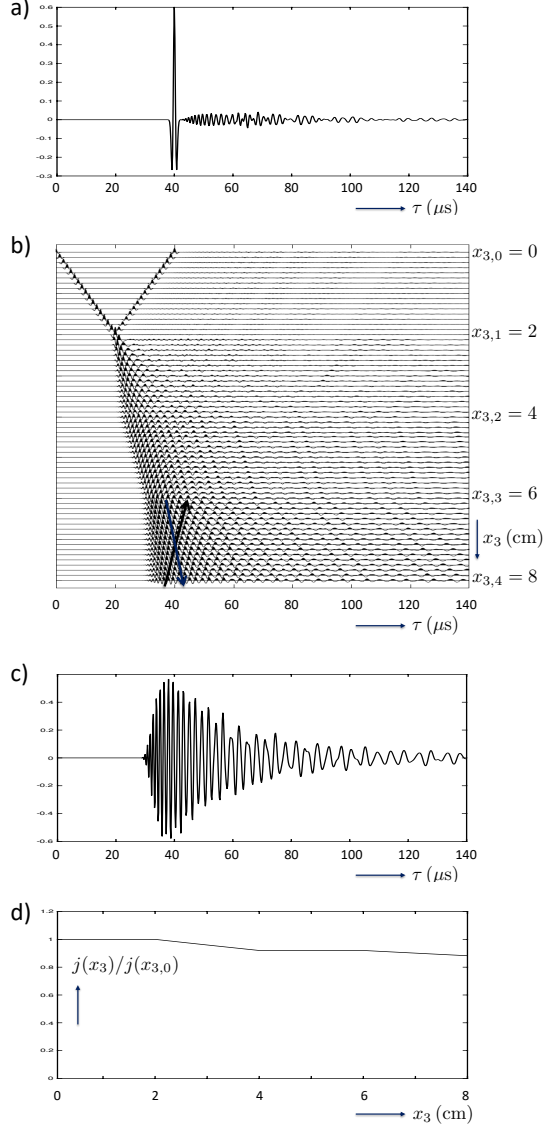


FIG. 7: Modelled wave field in the layered medium of Figure 6. (a) Reflection response  $R(s_1 = 0, x_{3,0}, \tau)$ . (b) Green's function  $G(s_1 = 0, x_3, x_{3,0}, \tau)$ . (c) Transmission response  $T(s_1 = 0, x_{3,4}, x_{3,0}, \tau)$ . (d) Power flux density as a function of  $x_3$ .

a time-dependent amplitude gain of  $\exp(2.5\tau/\tau_{\max})$ , with  $\tau_{\max} = 140 \mu\text{s}$ , has been applied in this display. This figure shows how the wave field propagates through the layers and scatters at the interfaces. The downward and upward pointing arrows in the deepest layer indicate the opposite group and phase propagation directions. The upward propagating part of the upper trace in this figure is proportional to the reflection response  $R(s_1 = 0, x_{3,0}, \tau)$  (see equation (54)), which is shown separately in Figure 7(a). Similarly, the lower trace is

proportional to the transmission response  $T(s_1 = 0, x_{3,4}, x_{3,0}, \tau)$ , with  $x_{3,4} = 8$  cm, which is shown separately in Figure 7(c). The trace at  $x_3 = 5$  cm is equal to the superposition of Figures 5(a) and (c). Figure 7(d) shows the power flux density  $j(x_3)$ , defined in equation (31), divided by  $j(x_{3,0})$ . In the DNG layers it decreases because  $\Gamma \neq 0$  in these layers. In a lossless medium  $j(x_3)$  would be constant, i.e., propagation invariant. Its deviation from being constant implies that the Marchenko method, which is based on propagation invariants, cannot lead to exact results.

We use the Marchenko method discussed in section IV to retrieve the Green's function  $G(s_1 = 0, x_3, x_{3,0}, \tau)$  inside the medium from the reflection response  $R(s_1 = 0, x_{3,0}, \tau)$ , shown in Figure 7(a). Apart from the reflection we response, we also need an estimate of the direct arrival of the focusing function,  $f_{1,d}^+(s_1 = 0, x_{3,0}, x_{3,F}, \tau)$ , which, according to equation (73), follows from the inverse of the direct arrival of the transmission response. For this direct arrival we need a background model of the medium. For the moment we use the exact model, but in a later example we replace it by an approximate model. Figure 8(a) shows  $f_{1,d}^+(s_1 = 0, x_{3,0}, x_3, -\tau)$  (convolved with  $S(\tau)$ ) for variable  $x_3$ . The trace at  $x_3 = 5$  cm is equal to Figure 5(b). Given the reflection response at the surface (Figure 7(a)), the direct arrival of the focusing function (Figure 8(a)), and the depth-dependent onset times  $\tau_{\text{on}}^+$  and  $\tau_{\text{on}}^-$ , we apply the iterative Marchenko scheme of equations (70) – (72) for 64 focal depths, ranging from  $x_{3,F} = 1.25$  mm to  $x_{3,F} = 8$  cm, with steps  $\Delta x_{3,F} = 1.25$  mm. For each focal depth  $x_{3,F}$  we apply 5 iterations. The obtained focusing functions  $f_1^-(s_1 = 0, x_{3,0}, x_{3,F}, \tau)$  and  $f_1^+(s_1 = 0, x_{3,0}, x_{3,F}, \tau)$  are subsequently used in equations (63) and (64) to obtain the Green's functions  $G^-(s_1 = 0, x_{3,F}, x_{3,0}, \tau)$  and  $G^+(s_1 = 0, x_{3,F}, x_{3,0}, \tau)$ . These are shown in Figures 8(b) and 8(c) for variable  $x_3$ . Superposing these results yields the total Green's function  $G(s_1 = 0, x_3, x_{3,0}, \tau)$ , see Figure 9(a). Figure 9(b) shows the difference of this retrieved Green's function with the directly modelled Green's function in Figure 7(b) (the same time-dependent amplitude gain has been applied as in the other figures). Note that the difference is overall small. From the decomposed Green's functions we can retrieve the reflection response  $R(s_1 = 0, x_3, \tau)$  for any  $x_3$  by inverting equation (74). The retrieved response  $R(s_1 = 0, x_{3,F}, \tau)$  for  $x_{3,F} = 5$  cm is shown in Figure 9(c). This is the reflection response of the third interface at  $x_{3,3} = 6$  cm in Figure 6, measured with a virtual source and a virtual receiver 1 cm above this interface. We observe a single primary reflection event at  $8.0 \mu\text{s}$ ; the multiple reflections occurring in the medium above  $x_{3,F}$  have been properly

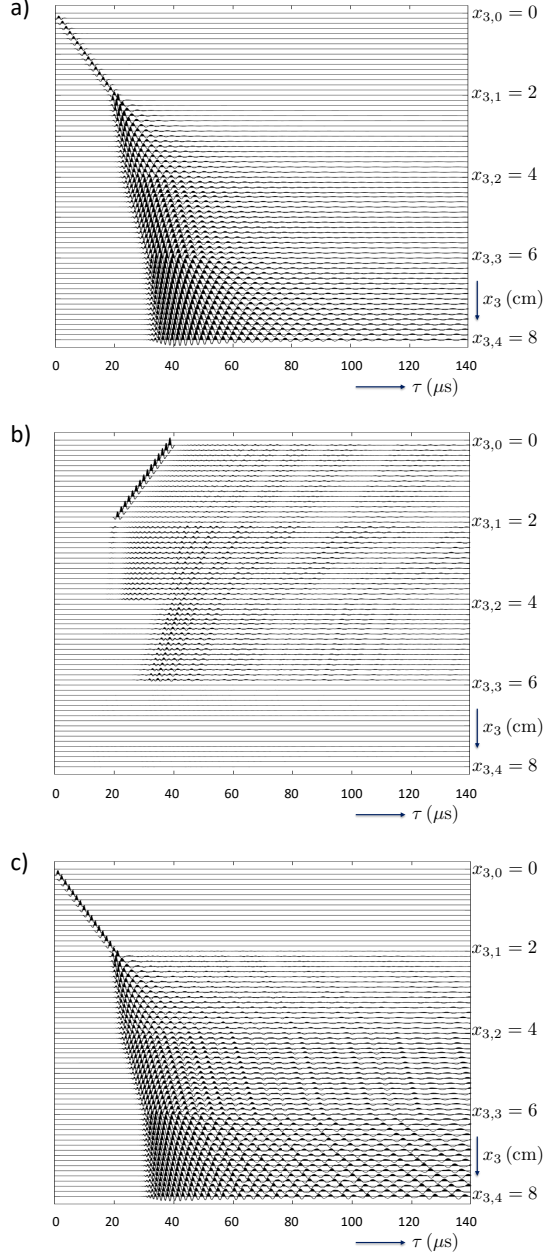


FIG. 8: *Wavefield retrieval with the Marchenko method. (a) Time-reversed direct arrival of the focusing function,  $f_{1,d}^+(s_1 = 0, x_{3,0}, x_3, -\tau)$ . (b) Retrieved upgoing Green's function  $G^-(s_1 = 0, x_3, x_{3,0}, \tau)$ . (c) Retrieved downgoing Green's function  $G^+(s_1 = 0, x_3, x_{3,0}, \tau)$ .*

removed (apart from a very small remnant of a multiple reflection at approximately 24.0  $\mu\text{s}$ ). The amplitude of the reflection event at 8.0  $\mu\text{s}$  is 0.159, which is a slight underestimation of the true reflection coefficient  $r_3 = 0.180$  for  $\omega = \omega_c$ . This discrepancy is due to the loss occurring in the DNG layer between  $x_{3,1} = 2$  cm and  $x_{3,2} = 4$  cm.

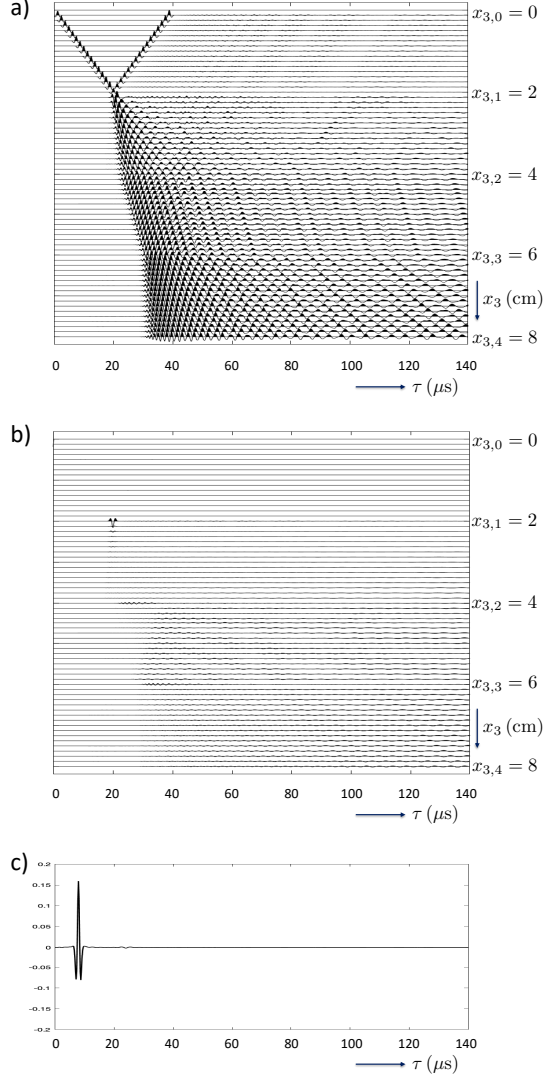


FIG. 9: *Wavefield retrieval with the Marchenko method (continued).* (a) *Total Green's function*  $G(s_1 = 0, x_3, x_{3,0}, \tau) = G^+(s_1 = 0, x_3, x_{3,0}, \tau) + G^-(s_1 = 0, x_3, x_{3,0}, \tau)$ . (b) *Difference of the retrieved Green's function with the directly modelled Green's function of Figure 7(b).* (c) *Retrieved reflection response at  $x_{3,F} = 5$  cm of the interface at  $x_{3,3} = 6$  cm.*

To emphasize what we have achieved with the Marchenko method we repeat this numerical experiment with a method that handles primaries only (to this end, we use the same method as before, but apply zero iterations for each focal depth). Figure 10(a) shows the retrieved Green's function  $G(s_1 = 0, x_3, x_{3,0}, \tau)$  and Figure 10(b) the difference with the directly modelled Green's function in Figure 7(b). Note that this difference is significantly stronger than that in Figure 9(b). Figure 10(c) shows the retrieved reflection response

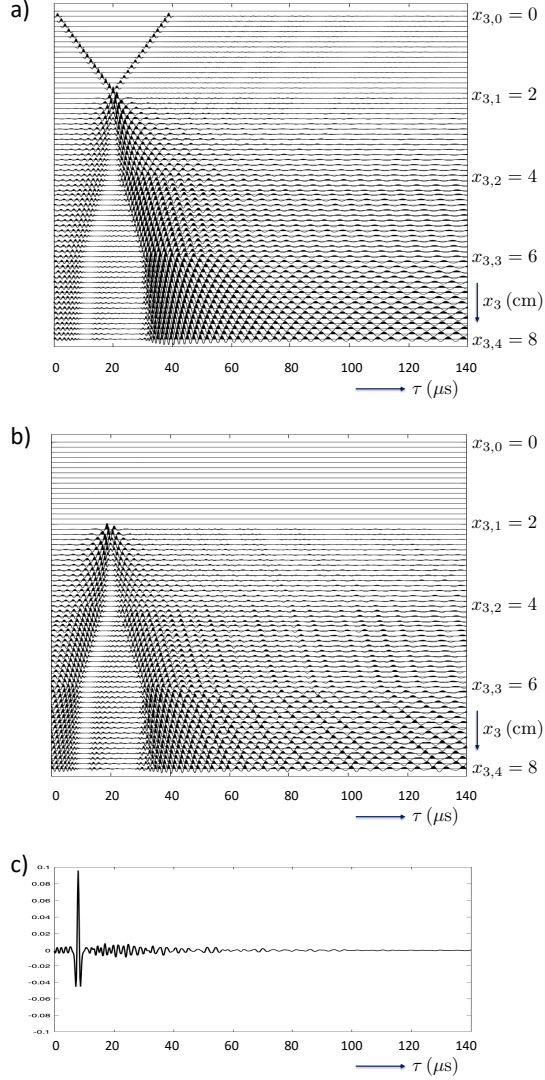


FIG. 10: As Figure 9, but using using a method that handles primaries only.

$R(s_1 = 0, x_{3,F}, \tau)$  for  $x_{3,F} = 5$  cm, obtained by inverting equation (74). The amplitude of the retrieved reflection event at  $8.0$   $\mu\text{s}$  is now  $0.096$ , almost a factor two too low. Moreover, the events directly following this reflection event are caused by multiple reflections in the medium above  $x_{3,F}$ , which obviously have not been removed by this method.

In practice we don't know the exact model, so we can obtain only an estimate of the direct arrival of the focusing function and of the onset times  $\tau_{\text{on}}^+$  and  $\tau_{\text{on}}^-$ . We apply the same Marchenko method as above (again with 5 iterations for each focal depth), but this time we use erroneous phase velocities  $c_0$  of  $975$ ,  $-2050$ ,  $2550$  and  $-1950$  m/s in the four layers (and the same numerical values for the mass density). Because of the erroneous velocities,

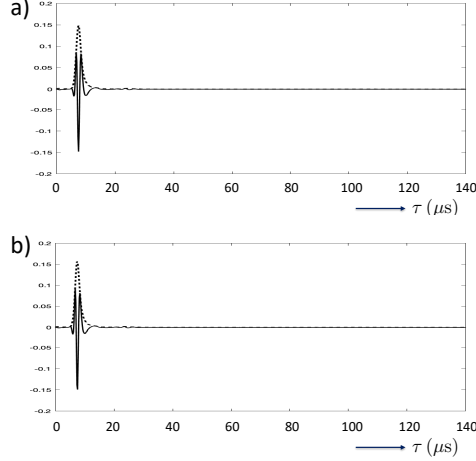


FIG. 11: (a) As Figure 9(c), but using erroneous phase velocities. (b) As Figure 9(c), but for  $s_1 = 40\mu\text{s}/\text{m}$  and using erroneous phase velocities.

the traveltimes of the retrieved Green's functions are erroneous as well, but the multiple reflections are correctly handled [62]. Figure 11(a) shows the retrieved reflection response  $R(s_1 = 0, x_{3,F}, \tau)$  for  $x_{3,F} = 5$  cm. We observe a single reflection event at  $7.6 \mu\text{s}$  and hardly any remnants of multiples, which confirms that the multiple reflections occurring in the medium above  $x_{3,F}$  have again been properly removed. The phase of the reflection event is distorted, but the envelope (indicated by the dashed line) has a peak value of 0.149, which still approximates the true reflection coefficient  $r_3 = 0.180$  reasonably well.

Finally, we repeat the numerical experiment, using the same erroneous phase velocities, for a dipping plane wave with a small non-zero horizontal slowness  $s_1 = 40\mu\text{s}/\text{m}$ . The propagation angle  $\alpha$  for  $\omega = \omega_c$  is related to the slowness  $s_1$  and the phase velocities  $c_0$  of the different layers via  $\alpha = \arcsin(s_1 c_0)$ . For  $s_1 = 40\mu\text{s}/\text{m}$ , the angles in the four layers of Figure 6 are  $2.29^\circ$ ,  $-4.59^\circ$ ,  $5.74^\circ$  and  $-6.89^\circ$ , respectively. The retrieved reflection response  $R(s_1 = 0, x_{3,F}, \tau)$  for  $x_{3,F} = 5$  cm is shown in Figure 11(b). The amplitude of the retrieved reflection response of the third interface is 0.157, which is a reasonable approximation of the true reflection coefficient  $r_3 = 0.181$  for  $\omega = \omega_c$  and  $s_1 = 40\mu\text{s}/\text{m}$ .

## VI. CONCLUDING REMARKS

We have shown that the Marchenko method, which retrieves the wavefield inside a medium from its reflection response at the surface, can be extended for metamaterials.

The method holds, in the low frequency limit, for elastodynamic and electromagnetic waves in layered media, consisting of a mix of natural materials and metamaterials. Multiple scattering between the layer interfaces is properly taken into account. We have shown with a numerical example that the method accurately retrieves the response to a source at the surface, observed by virtual receivers inside the medium. By deconvolving the retrieved upgoing field by the retrieved downgoing field, we accurately obtain the reflection response between a virtual source and a virtual receiver, both inside the medium.

The method works well for vertically propagating plane waves and for dipping plane waves with small horizontal slownesses, corresponding to propagation angles up to approximately  $7^\circ$ . For larger horizontal slownesses the method becomes unstable. Due to the strong dispersive behaviour of the DNG layers, the propagation angle for a fixed horizontal slowness is frequency-dependent and can quickly become post-critical for high frequencies, which explains the unstable behaviour. A possible remedy is to remove the high frequencies from the source spectrum, but this will go at the cost of resolution. Further research is needed to optimize the proposed method for a wider range of propagation angles.

The proposed method can potentially be used in any application of metamaterials where knowledge of the wavefield inside the medium is required, for example in non-destructive testing of layered materials, where anomalies of the retrieved reflectivity may be used to determine the precise location of a delamination.

### Acknowledgements

This work has received funding from the European Union's Horizon 2020 research and innovation programme: European Research Council (grant agreement 742703).

- 
- [1] V. A. Marchenko, Dokl. Akad. Nauk SSSR **104**, 695 (1955).
  - [2] G. L. Lamb, *Elements of soliton theory* (John Wiley and Sons, Inc., New York, 1980).
  - [3] K. Chadan and P. C. Sabatier, *Inverse problems in quantum scattering theory* (Springer, Berlin, 1989).
  - [4] D. E. Budreck and J. H. Rose, Inverse Prob. **6**, 331 (1990).
  - [5] J. H. Rose, Phys. Rev. A **65**, 012707 (2001).

- [6] J. H. Rose, *Inverse Prob.* **18**, 1923 (2002).
- [7] F. Brogгинi and R. Snieder, *Eur. J. Phys.* **33**, 593 (2012).
- [8] K. Wapenaar, F. Brogгинi, and R. Snieder, *Geophys. J. Int.* **190**, 1020 (2012).
- [9] J. Van der Neut, I. Vasconcelos, and K. Wapenaar, *Geophys. J. Int.* **203**, 792 (2015).
- [10] P. Elison, D. J. van Manen, J. O. A. Robertsson, M. S. Dukalski, and K. de Vos, *Geophys. J. Int.* **215**, 1118 (2018).
- [11] K. Wapenaar, J. Brackenhoff, J. Thorbecke, J. van der Neut, E. Slob, and E. Verschuur, *Sci. Rep.* **8**, 2497 (2018).
- [12] M. Dukalski and K. de Vos, *Geophys. J. Int.* **212**, 760 (2018).
- [13] J. Brackenhoff, J. Thorbecke, and K. Wapenaar, *Solid Earth* **10**, 1301 (2019).
- [14] K. Wapenaar, J. Thorbecke, J. van der Neut, F. Brogгинi, E. Slob, and R. Snieder, *Geophysics* **79**, WA39 (2014).
- [15] E. Slob, K. Wapenaar, F. Brogгинi, and R. Snieder, *Geophysics* **79**, S63 (2014).
- [16] F. Brogгинi, R. Snieder, and K. Wapenaar, *Geophysics* **79**, WA107 (2014).
- [17] G. A. Meles, K. Löer, M. Ravasi, A. Curtis, and C. A. da Costa Filho, *Geophysics* **80**, A7 (2015).
- [18] M. Ravasi, I. Vasconcelos, A. Kritski, A. Curtis, C. A. da Costa Filho, and G. A. Meles, *Geophys. J. Int.* **205**, 99 (2016).
- [19] J. Van der Neut, M. Ravasi, Y. Liu, and I. Vasconcelos, *Geophysics* **82**, Q53 (2017).
- [20] C. Mildner, F. Brogгинi, J. O. A. Robertsson, D. J. van Manen, and S. Greenhalgh, *Geophysics* **82**, R75 (2017).
- [21] M. Ravasi, *Geophysics* **82**, S439 (2017).
- [22] M. Staring, R. Pereira, H. Douma, J. van der Neut, and K. Wapenaar, *Geophysics* **83**, S579 (2018).
- [23] K. Wapenaar and C. Reinicke, *J. Acoust. Soc. Am.* **146**, 810 (2019).
- [24] V. G. Veselago, *Soviet Physics Uspekhi* **10**, 509 (1968).
- [25] J. B. Pendry, *Phys. Rev. Lett.* **85**, 3966 (2000).
- [26] R. W. Ziolkowski and E. Heyman, *Phys. Rev. E* **64**, 056625 (2001).
- [27] R. Marqués, F. Medina, and R. Rafii-El-Idrissi, *Phys. Rev. B* **65**, 144440 (2002).
- [28] R. W. Ziolkowski and A. D. Kipple, *Phys. Rev. E* **68**, 026615 (2003).
- [29] R. W. Ziolkowski, *Opt. Express* **11**, 662 (2003).

- [30] N. Engheta and R. W. Ziolkowski, *Metamaterials: Physics and Engineering Explorations* (John Wiley and Sons, Inc., 2006).
- [31] D. R. Smith and J. B. Pendry, *J. Opt. Soc. Am. B* **23**, 391 (2006).
- [32] N. Yu, P. Genevet, M. A. Kats, F. Aieta, J.-F. Tetienne, F. Capasso, and Z. Gaburro, *Science* **334**, 333 (2011).
- [33] J. R. Willis, *Proc. R. Soc. A* **467**, 1865 (2011).
- [34] J. Nemirovsky, M. C. Rechtsman, and M. Segev, *Opt. Express* **20**, 8907 (2012).
- [35] Z. Liu, X. Zhang, Y. Mao, Y. Y. Zhu, Z. Yang, C. T. Chan, and P. Sheng, *Science* **289**, 1734 (2000).
- [36] Z. Liu, C. T. Chan, and P. Sheng, *Phys. Rev. B* **71**, 014103 (2005).
- [37] S. Guenneau, A. Movchan, G. Pétursson, and S. A. Ramakrishna, *New J. Phys.* **9**, 399 (2007).
- [38] A. N. Norris, *J. Acoust. Soc. Am.* **125**, 839 (2009).
- [39] J. R. Willis, *C. R. Mec.* **340**, 181 (2012).
- [40] R. Zhu, X. N. Liu, G. L. Huang, H. Huang, and C. T. Sun, *Phys. Rev. B* **86**, 144307 (2012).
- [41] A. P. Liu, R. Zhu, X. N. Liu, G. K. Hu, and G. L. Huang, *Wave Motion* **49**, 411 (2012).
- [42] A. N. Norris, A. L. Shuvalov, and A. A. Kutsenko, *Proc. R. Soc. A* **468**, 1629 (2012).
- [43] Z. Liang and J. Li, *Phys. Rev. Lett.* **108**, 114301 (2012).
- [44] M. R. Haberman and M. D. Guild, *Phys. Today* **69**, 42 (2016).
- [45] H. Nassar, H. Chen, A. N. Norris, M. R. Haberman, and G. L. Huang, *Proc. R. Soc. A* **473**, 20170188 (2017).
- [46] W. T. Thomson, *J. Appl. Phys.* **21**, 89 (1950).
- [47] N. A. Haskell, *Bull. Seismol. Soc. Am.* **43**, 17 (1953).
- [48] J. P. Coronas, *J. Math. Anal. Appl.* **50**, 361 (1975).
- [49] B. Ursin, *Geophysics* **48**, 1063 (1983).
- [50] L. Fishman and J. J. McCoy, *J. Math. Phys.* **25**, 285 (1984).
- [51] M. V. de Hoop, *J. Math. Phys.* **37**, 3246 (1996).
- [52] K. Wapenaar, *Geophys. J. Int.* **216**, 560 (2019).
- [53] A. J. Haines, *Geophys. J. Int.* **95**, 237 (1988).
- [54] B. L. N. Kennett, K. Koketsu, and A. J. Haines, *Geophys. J. Int.* **103**, 95 (1990).
- [55] K. Koketsu, B. L. N. Kennett, and H. Takenaka, *Geophys. J. Int.* **105**, 119 (1991).
- [56] H. Takenaka, B. L. N. Kennett, and K. Koketsu, *Wave Motion* **17**, 299 (1993).

- [57] K. Wapenaar, F. Broggini, E. Slob, and R. Snieder, *Phys. Rev. Lett.* **110**, 084301 (2013).
- [58] P. L. Stoffa, *Tau-p - A plane wave approach to the analysis of seismic data* (Kluwer Academic Publishers, Dordrecht, 1989).
- [59] K. Wapenaar, J. Fokkema, M. Dillen, and P. Scherpenhuijsen, in *SEG, Expanded Abstracts* (2000), pp. 2377–2380.
- [60] L. Amundsen, *Geophysics* **66**, 327 (2001).
- [61] B. L. N. Kennett and N. J. Kerry, *Geophys. J. R. Astron. Soc.* **57**, 557 (1979).
- [62] K. Wapenaar, J. Thorbecke, J. van der Neut, F. Broggini, E. Slob, and R. Snieder, *J. Acoust. Soc. Am.* **135**, 2847 (2014).